KSCE Journal of Civil Engineering (2021) 25(2):404-416
DOI 10.1007/s12205-020-0349-y

pISSN 1226-7988, eISSN 1976-3808
www.springer.com/12205

Geotechnical Engineering

Deformation and Stability Analysis of Embankment over Stone Column-Strengthened Soft Ground

Ali Ghorbani[a], **Iman Hosseinpour**[a], **and Mehdi Shormage**[a]

[a]*Civil Engineering Department, Faculty of Engineering, University of Guilan, Rasht, Iran*

ARTICLE HISTORY

Received 26 February 2020
Revised 12 June 2020
Accepted 14 September 2020
Published Online 4 December 2020

KEYWORDS

Geosynthetics
Soft soil
Stone column
Embankment
Numerical analysis

ABSTRACT

Compacted granular columns are commonly used to support embankments over soft soils. Using a reinforcement layer under the embankment causes the total stress to be further transferred to the column rather than soft soil, thus reducing total deformations of the subsoil. In this paper two dimensional (2D) numerical analysis was used to study the influence of stone columns and basal geosynthetic on deformations and stability of an embankment over soft deposit by means of Plaxis 2D finite element code. Unit cell to plane strain conversion approach was applied to transform columns into equivalent walls thus allowing to simulate a full embankment over a group of columns. Comprehensive parametric analysis was then performed to investigate the role of different critical parameters on embankment behavior. Results showed that the use of stone columns yielded the total deformations of the subsoil to significantly reduce, while its influence was less remarkable as a high stiffness geogrid was placed under the embankment. It was also found that the stone column length was the most influential parameter on the embankment total deformations, so that increasing columns length from 0.25Hs to 0.75Hs reduced the vertical and horizontal deformations by about two and five times, respectively. In addition, the use of a high stiffness basal geogrid caused the stability of the embankment to remarkably improve as the value of safety factor at the end of construction increased from 1.25 to about 1.9.

1. Introduction

Lands composed of soft, saturated sediment layers are problematic due to their low shear strength and high compressibility. The increasing population and lack of suitable ground have inevitably led to the usage of such weak deposits for constructions. Consequently, the application of various soil improvement methods is essential when faced with soft or very soft soils (Mitchell and Huber, 1985; Alfaro et al., 1994).

Among various methods available to improve soft soils (e.g., vertical drains, sand wicks, chemical additives, reinforcement, surcharge and vacuum preloading, etc.) ground improvement with an emphasis on the granular column technology overcomes construction problems by reducing the settlement under loading and speeding up the consolidation process (Hosseinpour et al., 2010; Han, 2015b; Al-Bared and Marto, 2017; Mohapatra and Rajagopal, 2017; Almeida et al., 2018; Mahawish et al., 2018; Kadhim et al., 2018; Al-Bared et al., 2019; Lima et al., 2019; Xue et al., 2019). The existence of the granular columns creates a composite material stiffer than the virgin weak soil, which attains its load capacity from the confinement provided by the surrounding soil (Greenwood, 1970; Poorooshasb and Meyerhof, 1997; Han, 2015a; Almeida et al., 2019; Samanta and Bhowmik, 2019). In addition, owing to the high drainage capability of the aggregates, the use of granular columns has attracted considerable attention. Therefore, it can be also utilized to reduce liquefaction potential in loose soils (Cengiz et al., 2019).

In practice, it is common to use a 50 – 100 cm thick compacted granular blanket to facilitate the implementation of stone columns on very soft grounds. While this firm layer provides surface drainage, it is also effective in redistributing and transferring embankment stress to the stone columns under the arching phenomenon. This dense layer can be further reinforced with a geosynthetic layer on top (often geogrid) which subsequently results in a significant increase of the bearing capacity due to its high tensile stiffness as well as considerable interlocking with

CORRESPONDENCE Ali Ghorbani ghorbani@guilan.ac.ir Civil Engineering Department, Faculty of Engineering, University of Guilan, Rasht, Iran

granular materials. Furthermore, the membrane effect of the geosynthetic layer reduces the stress transferred to soft soil, thereby reducing its total deformations (Márcio de Souza and Marques, 2013; Han, 2015b; Hosseinpour et al., 2019).

Numerous researchers have investigated the behavior of stone columns used to strengthen soft clay using laboratory experiments, numerical tools, and analytical methods. Results demonstrated that the use of stone column significantly reduces the total stress imposed on the soft clay bed as well as the consolidation settlement (Najjar et al., 2010; Indraratna et al., 2013; Basack et al., 2016; Debnath and Dey, 2017; Golait and Padade, 2017; Hosseinpour et al., 2017a; Mehrannia et al., 2018; Sharma, 2019).

Abusharar and Han (2011) studied the safety factor of an embankment on soft soil using the two-dimensional finite element method. The results revealed that increasing the distance between stone columns and the thickness of the soft clay decreased the safety factor. Moreover, it was observed that increasing the diameter of the columns and the cohesion of the soft clay improved embankment stability.

Indraratna et al. (2015) studied the deformation of stone columns under static loading on soft soil using finite difference method (FDM). The results showed that increasing the diameter of column reduced its lateral deformation which, in turn, increased the failure stress of the composite soil-stone column foundation.

Zhao et al. (2019) evaluated numerically the effect of different parameters on stress concentration on stone columns. Their investigations showed that increasing the distance between the stone columns increased the concentration of stress in the columns as well as the tensile force in the basal geogrid. In addition, they found that using basal geogrid and increasing the modulus of elasticity of both the stone column and the surrounding soft soil increased the bearing capacity.

As reported, the majority of the previous numerical analyses studied the behavior of a single stone column in the axial symmetry configuration (i.e., unit cell approach). Although the use of a unit cell model yields acceptable results when estimating the settlement and distribution of stress under the embankment, the horizontal deformation at the embankment toe or at any distance from the toe cannot be calculated. This is due to the application of horizontal constraints along the side borders which prevents the occurrence of horizontal deformations in the unit cell model. Moreover, the horizontal fixities embedded in the side borders of the unit cell prevent the basal geosynthetic to deform horizontally thus leading to a negligible value of the geosynthetic tensile force compared to the reality.

To overcome these limitations, the axisymmetric to plane strain conversion methodology proposed by Tan et al. (2008) is employed allowing to analyze full embankment over a group of stone columns. In this contribution, the stone column is replaced by an extended wall with a reduced thickness, while the center-to-center distance of columns remains constant. Initially, the verification of the proposed model is examined using the above method. Then, the behavior of embankment and soft clay foundation is studied by changing the properties of the stone column, and the soft clay layer.

2. Plane Strain Configuration

Tan et al. (2008) proposed two methods to convert the geometry of a single-stone column from a three-dimensional into a two-dimensional plane strain. In both methods, the spacing between stone columns is maintained and each stone column is replaced by an extended shear wall. In the first method, the thickness of the wall is equal to the diameter of the stone column, and the soil permeability changes according to correlation equations. However, in the second method, the permeability of soil materials remains constant while the thickness of the wall is accordingly reduced. Both methods are validated relative to the field data; subsequently, only the second method yielded valid satisfactory results. Therefore, in this study, the second methodology proposed by Tan et al. (2008) is employed here in order to model the group of stone columns. Fig. 1 demonstrates a single-stone column conversion into an equivalent shear wall where the thickness of the shear wall is calculated as follows:

$$b_c = B\frac{r_c^2}{R^2}, \tag{1}$$

where R is the influence radius of the stone column at the symmetrical condition, and B is the influence radius in the plane-strain condition. The value of R depends on the arrangement of stone columns (i.e., square or triangular), as well as the center-to-center distance of stone columns. For the columns installed into a square grid, the value of R is 1.13S where S is the center-to-center spacing between stone columns.

3. Model Validation

The results of instrumentation for a real highway embankment in Malaysia in 2003 (reported in Tan and Oo, 2005) were used to validate the numerical model. Fig. 2 represents the cross-sectional view of the embankment and the subsoil profile. As can

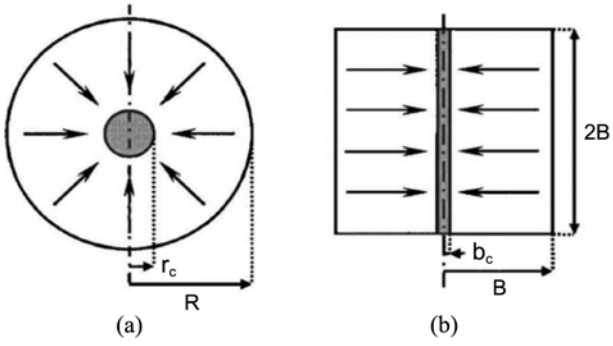

Fig. 1. Geometry Conversion of Stone Column from Axial Symmetry to Plane Strain (Tan et al., 2008): (a) Axisymmetric, (b) Plane Strain, Method 2

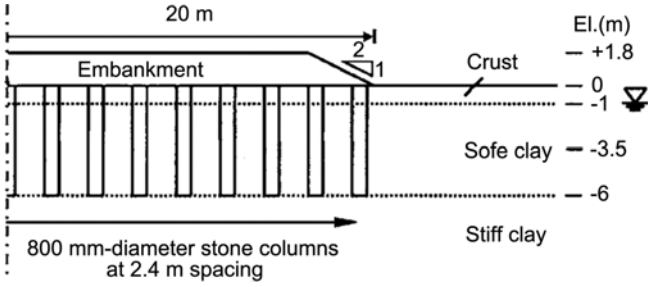

Fig. 2. Cross Sectional View of Embankment Used for Model Validation (Tan et al., 2008)

be seen, the embankment is 40 m wide at the base and its height is 1.8 m with a side slope of 1V-2H. The 80 cm diameter stone columns were installed in a square grid with center-to-center spacing of 2.4 m covering to a depth of 6 m below the ground surface. Moreover, a 1 m thick dense granular soil layer was placed on top of the soft clay to improve drainage conditions and construction operations on soft soil. To understand the behavior of the embankment and the soil beneath, a set of instruments was used to monitor the variations of settlements right at the center of the embankment and the pore water pressure in the middle of the clay layer.

Plaxis 2D, V.8.5 finite element code (Brinkgreve and Vermeer, 2012) was employed for the numerical analysis of embankment due to its capability of conducting coupled consolidation analyses, as it has been extensively used by several researchers (Elsawy, 2013; Hosseinpour et al., 2017b; Muzammil et al., 2018; Vinoth et al., 2019).

Figure 3(a) shows the numerical model adopted to perform the validation analysis. Due to the axial symmetry at the center, only half of the embankment is simulated. The dimensions of embankment and clay bed as well as the stone columns are identical to those of the actual fieldwork reported by Tan et al. (2008). Given the plane strain conditions, stone columns are modeled using continuous walls, with the thickness calculated via Eq. (1). According to the center-to-center distance between stone columns of 2.4 m and their diameter of 0.8 m, the equivalent thickness of walls in the plane strain model is obtained as 21 cm. Subsequently, the boundary conditions are applied in a manner that the side borders of the model would only have vertical movement, while the model is entirely fixed at the base.

To achieve accurate results, the model was meshed using 15-nodes triangular elements. Consequently, the model is divided into 960 elements along with 7,853 and 11,520 nodes to calculate either strains or changes in stresses at any different locations. Since the finite element results are sensitive to the mesh coarseness, a series of sensitivity analyses was performed to obtain the most accurate results. According to the results, a fine mesh coarseness was found to provide the most accurate prediction of the measured data and thus assigned to generate the model into triangular elements. Fig. 3(b) shows the applied boundaries as well as a mesh generated model.

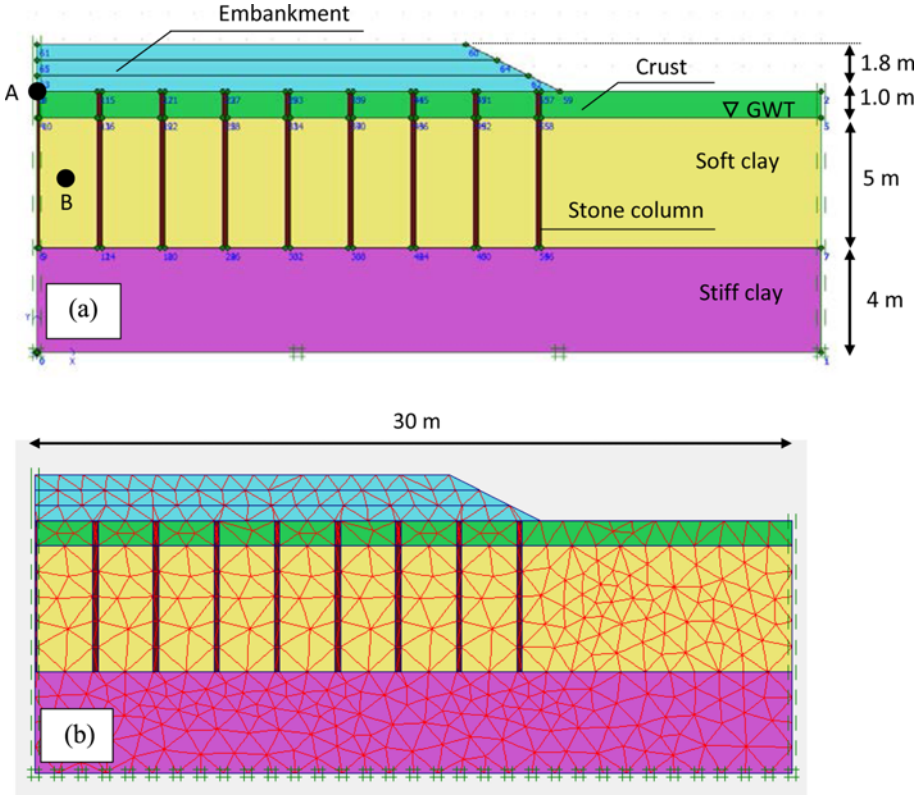

Fig. 3. Two-Dimensional Plane Strain Model of Embankment: (a) Numerical Model Used for Analysis, (b) Mesh Generation

Table 1. Properties of Soil Materials (adopted from Tan et al., 2008)

Material	γ_{dry} (kN/m^3)	γ_{sat} (kN/m^3)	ν' (–)	E (MPa)	k_h (m/s)	k_v (m/s)	c' (kPa)	ϕ (deg)
Embankment fill	18	20	0.3	15	1.16*	1.16*	3	33
Crust	17	18	0.3	15	3.47*	1.16*	3	28
Soft clay	15	15	0.3	1.1	3.47*	1.16*	1	20
Stiff clay	18	20	0.3	40	3.47*	1.16*	3	30
Stone column	19	20	0.3	30	1.16*	1.16*	5	40

The reinforcement was modeled as an isotropic geogrid element, available simply in Plaxis 2D, composing of six nodal triangular elements with three translational degrees of freedom per node. By assigning 15-node elements to soil materials, the geogrid is automatically simulated by a 5-node linear element. The geogrid element only has tensile stiffness and thus it can sustain tensile force along the length. A perfect bounding was assigned along with the interface between the geogrid element and the surrounding soil (Hatami and Bathurst, 2005; Tandel et al., 2012). The use of an elastic element inherently leads that the tensile rupture of the geosynthetic will not occur in the parametric study. Since the geogrid is only capable of sustaining tensile stress, only a tensile stiffness will be required to simulate its behavior, the value of which will be varied in parametric analyses.

Concerning constitutive models, the behavior of all types of soil materials is simulated using the elastic-plastic Mohr-Coulomb model, the parameters of which are presented in Table 1.

The embankment construction was performed in three stages, at each 60 cm thick fill was placed in three days. Consequently, the embankment was completed over a period of 9 days and reached a height of 1.8 m. Following the completion of loading, i.e., complete construction of embankment, a consolidation analysis is carried out and calculations are continued until complete dissipation of the excess pore water pressure.

Figure 4(a) compares variations of the measured and simulated settlements over time, for a point located below the embankment centerline (see point A in Fig. 3(a)). As can be seen, the numerical analysis could predict fairly well the trend and magnitude of the measured settlement with about 80 cm consolidation settlement occurred over a period of approximately 100 days.

In addition, Fig. 4(b) shows the distribution of pore water pressure at the center of the soft clay layer at point B. Based on this figure, the pore water pressure increasingly rises during the construction of the embankment (i.e., 9 days). Following, the pore pressure starts to dissipate gradually while it is disappeared over a period of 100 days, denoting the occurrence of a total consolidation. As can be observed, there is a good agreement between numerical results and field measurements confirming the adopted model is perfectly able to predict the embankment behavior. Therefore, the model can be employed to conduct parametric analyses to gain a better understanding of embankment behavior by changing some critical parameters.

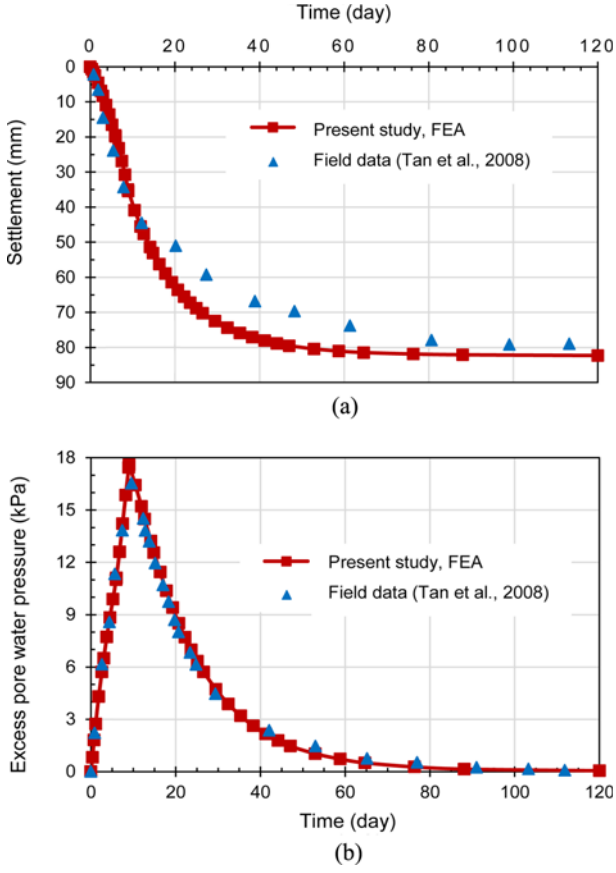

Fig. 4. Comparison of Numerical Results and Measurements: (a) Settlement Variations at Point A, (b) Changes in Excess Pore Water Pressure at Point B

4. Parametric Study

The behavior of the embankment was studied by changing parameters including the spacing between stone columns (S), basal geogrid stiffness (J), friction angel of soft clay bed (ϕ_s), stone column friction angle (ϕ_c) and stone column length (L_c) with their values listed in Table 2. It is noticed that the adopted parameters are in the range recommended by manuals and well-known reference textbooks e.g., Barksdale and Bachus (1983), Mitchell and Huber (1985), Almeida et al. (2019), Han (2015a).

It is also noted that, to achieve better performance and reveal the geogrid effect on parametric analyses, the height of the embankment and its density increase to 6 m and 20 kN/m^3,

Table 2. Variable Considered for Parametric Analysis

Parameter	Value	Unit
Spacing between the stone columns (S)	1.8, 2.0, 2.2, 2.4	(m)
Basal geogrid stiffness (J)	0, 4000	(kN/m)
Friction angle of the soft clay (ϕ_s)	20, 23, 26, 29	(degree)
Friction angle of the stone columns (ϕ_c)	38, 40, 42, 44	(degree)
Length of the stone columns (L_c)	0.25 H_s, 0.5 H_s, 0.75 H_s s, H_s*	---

*H_s is the thickness of soft clay layer.

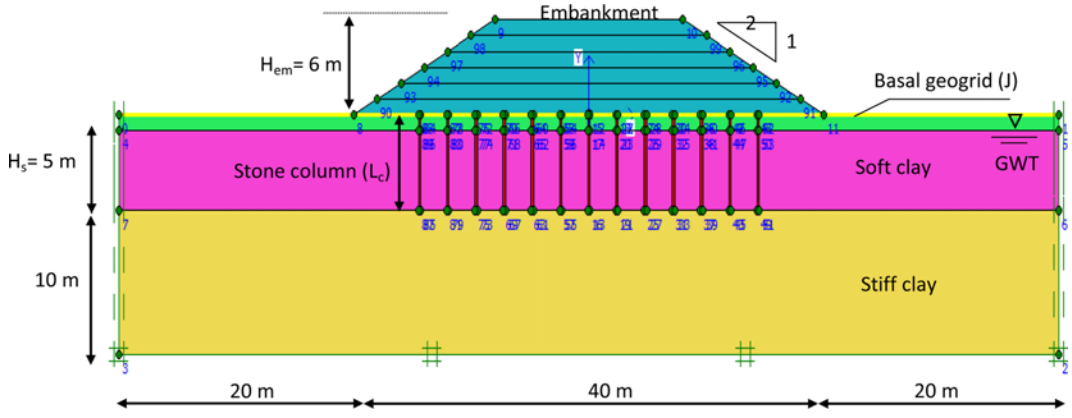

Fig. 5. Numerical Model Adopted for Parametric Study

respectively. The embankment is also placed over a period of 24 days, and consolidation analysis continues until the excess pore water pressure is dissipated. Fig. 5 shows the embankment geometry to be used in parametric analyses.

5. Results and Discussions

5.1 Influence of Spacing between the Stone Columns (S)

Figure 6(a) shows variations of the settlement profile under the unreinforced embankment for different spacing between stone columns. It is clearly seen that decreasing the spacing between columns significantly reduces the amount of settlement under the embankment. For example, by reducing the distance from 2.4 to 1.8 m, the maximum settlement below the embankment decreases by approximately 25%, i.e., from 470 to 350 mm. In addition, it is observed that reduction of spacing between the stone columns remarkably affects the amount of heave at the embankment toe. For instance, reduction of spacing between the columns from 2.4 to 1.8 m results in a complete removal of 112 mm heave at the embankment toes.

According to Fig. 6(b), when using a basal geogrid with stiffness of 4,000 kN/m, reducing the spaces between the stone columns from 2.4 to 1.8 m only reduces the maximum settlement from 470 to 420 mm, i.e., 10%. This behavior reflects the slight effect of changing the spacing between the stone columns when a very high-stiffness geogrid is placed under the embankment. Alternatively, the geogrid has a significant effect on the reduced heave at the embankment toe. As shown, given a constant spacing value of 2.4 m between stone columns, the magnitude of

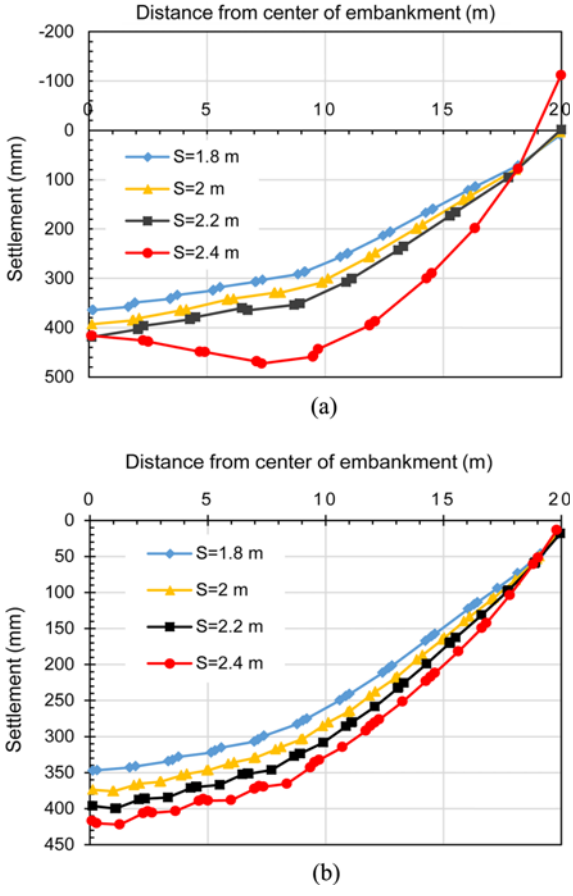

Fig. 6. Settlement Profile under the Embankment: (a) Unreinforced Embankment, (b) Reinforced Embankment with Basal Geogrid (J = 4,000 kN/m)

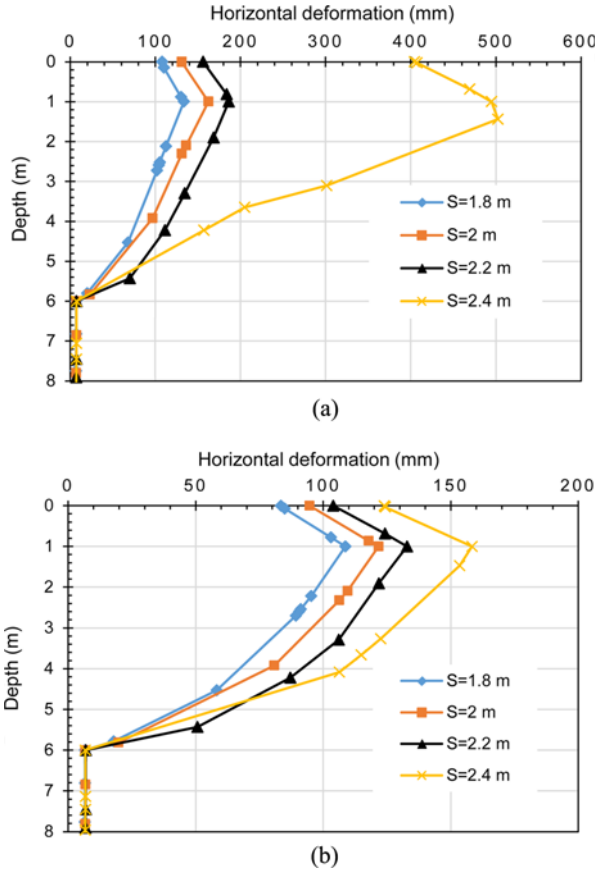

Fig. 7. Profile of the Soil Horizontal Deformation under the Embankment Toe: (a) Unreinforced Embankment, (b) Reinforced Embankment (J = 4,000 kN/m)

heave lowered from 112 mm to zero when a basal geogrid with stiffness of 4,000 kN/m is used.

Figure 7 shows the horizontal deformation profile of the foundation soil at the embankment toe for different spacing between the stone columns. According to Fig. 7(a), when the distance between the stone columns reduces, the maximum value of horizontal deformation of the foundation soil considerably decreases. For example, when the distance between the stone columns for unreinforced embankment decreases from 2.4 to 1.8 m, the maximum horizontal displacement reduces by approximately 73%, i.e. from 500 to 135 mm.

The significant rate of change in horizontal deformation when the column spacing is 2.4 m is due to the largest distance of the outer stone columns from the embankment toes, where the horizontal deformation is calculated. Since 2.4 m spaced stone columns offer negligible passive support to the soft soil underneath the embankment toe, the soil lateral deformation will be considerably higher in that case, compared to others.

As illustrated in Fig. 7(b), when a basal geogrid with stiffness of 4,000 kN/m is used, the effect of spacing between the stone columns on the maximum horizontal deformation of the subsoil is not as such as remarkable for the unreinforced embankment. For example, for the reinforced embankment when the column

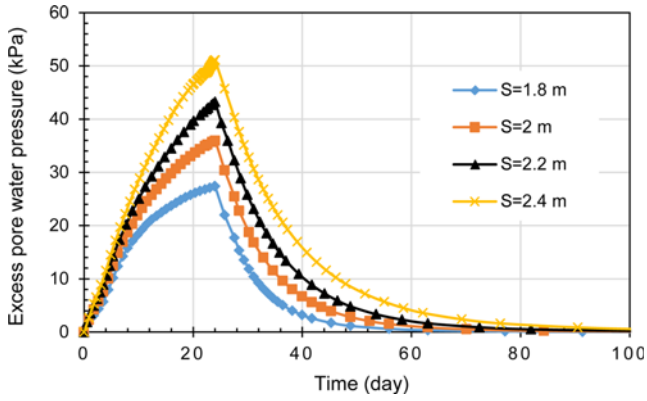

Fig. 8. Changes in Excess Pore Water Pressure in the Middle of the Clay Layer

spacing reduces from 2.4 to 1.8 m, the maximum horizontal displacement decreases by approximately 32%, i.e., from 160 to 110 mm.

Therefore, as pointed out in Johnson (2012), it can be concluded that the use of basal geogrid will have a significant influence on controlling the horizontal deformations of the subsoil, regardless of the spacing between the stone columns.

Figure 8 demonstrates variations of the excess pore water pressure versus time in the middle of the clay layer for different spacing between the stone columns. Based on this figure, spacing between the stone columns has a significant effect on maximal excess pore water pressure. It is seen that reducing the column spacing from 2.4 to 1.8 m decreases the maximum amount of excess pore pressure from 51 to 27 kPa. Moreover, given the following figure, the close-spaced stone columns considerably accelerate consolidation. This behavior can be interpreted by two reasons: first, a closer installed stone columns reduces the amount of the embankment total stress transferred to the soft soil thus the maximal excess pore pressure decreases (Almeida et al., 2018). Secondly, reducing the spacing between the stone columns shortens the radial flow path thus time to pore pressure dissipation significantly decreases.

5.2 Influence of the Friction Angle of Soft Clay Layer (ϕ_s)

Figure 9 shows the effect of the soft clay friction angle on the settlement profile under both reinforced and unreinforced embankments. In these analyses, the center-to-center distance between the stone columns was fixed at 2.4 m, while the soft clay friction angle was changed between the values listed in Table 2. According to Fig. 9(a) with respect to the unreinforced embankment, when the friction angle of the soft clay increases from 20° to 29°, both the maximum settlement and the heave at embankment toe decrease. As expressed by the change in the friction angle, the maximum settlement under embankment reduces by approximately 12%, i.e., from 475 to 420 mm, and the heave value diminishes from 110 mm to zero.

According to Fig. 9(b), for the embankment reinforced by a geogrid layer with stiffness of 4,000 kN/m, increasing the soft

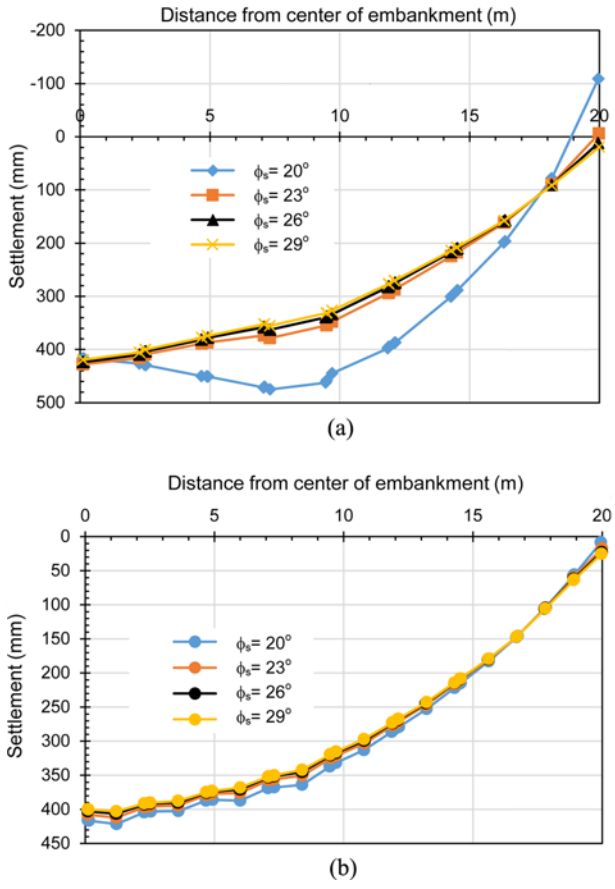

Fig. 9. Influence of the Friction Angle of the Clay Layer on Settlement Profile: (a) Unreinforced Embankment, (b) Reinforced Embankment with Basal Geogrid (J = 4,000 kN/m)

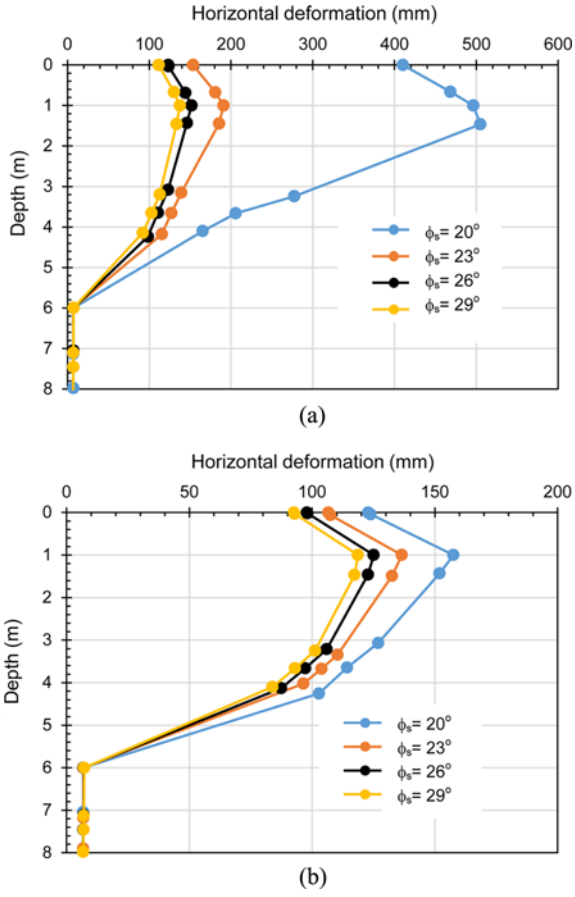

Fig. 10. Profile of the Soil Horizontal Deformation under the Embankment Toe: (a) Unreinforced Embankment, (b) Reinforced Embankment (J = 4,000 kN/m)

clay friction angle does not significantly affect neither the settlement under the embankment nor the heave at the embankment toes. Accordingly, it can be concluded that the effect of increasing the clay friction angle on embankment settlement and toe heave highly depends on the stiffness of the basal geogrid placed under the embankment.

The horizontal deformation profile of the foundation soil at the embankment toe for different friction angles of the soft clay layer is plotted in Fig. 10. Based on Fig. 10(a), when the clay friction angle increases, the maximum value of the horizontal deformation of subsoil considerably decreases. For example, when the friction angle of the soft clay underneath unreinforced embankment increases from 20° to 29°, the maximum horizontal displacement reduces by approximately 72%, i.e., from 504 to 137 mm.

According to Fig. 10(b), if a geogrid with a stiffness of 4,000 kN/m is used, the effect of increasing the clay friction angle on the maximum horizontal deformation of subsoil will not be significant. For instance, for the embankment reinforced by geogrid with a stiffness of 4,000 kN/m, increasing the clay friction angle from 20° to 29°, results the maximum horizontal displacement to reduce by almost 25%, i.e., from 157 to 118 mm. As a result, the effect of increased soft clay friction angle on the reduction of total deformations of unreinforced embankment is far more significant than embankment reinforced with high-stiffness geogrid.

Additionally, the significant effect of geogrid on reducing the maximum soil horizontal displacement can be understood in the following two figures. For example, for a given clay bed friction angle of 20°, the maximum soil horizontal displacement reduces by approximately 69%, i.e., from 504 to 157 mm, when a geogrid with stiffness of 4,000 kN/m is placed at the base of the embankment. Therefore, it could be concluded that the use of basal geogrid below the embankment has a significant effect on controlling the horizontal deformations of soft foundation.

Figure 11(a) shows variations of excess pore pressure in the middle of the soft clay layer for different values of the clay friction angle under unreinforced embankment. As can be seen, any change in the clay friction angle has no effect on the maximum excess pore pressure nor the time required for reaching complete consolidation. Variations of the total vertical stresses on the stone column and the soft clay layer could be useful to interpret this behavior.

Figure 11(b) demonstrates variations of the total stress transferred to the top of the central stone column and the surrounding clay,

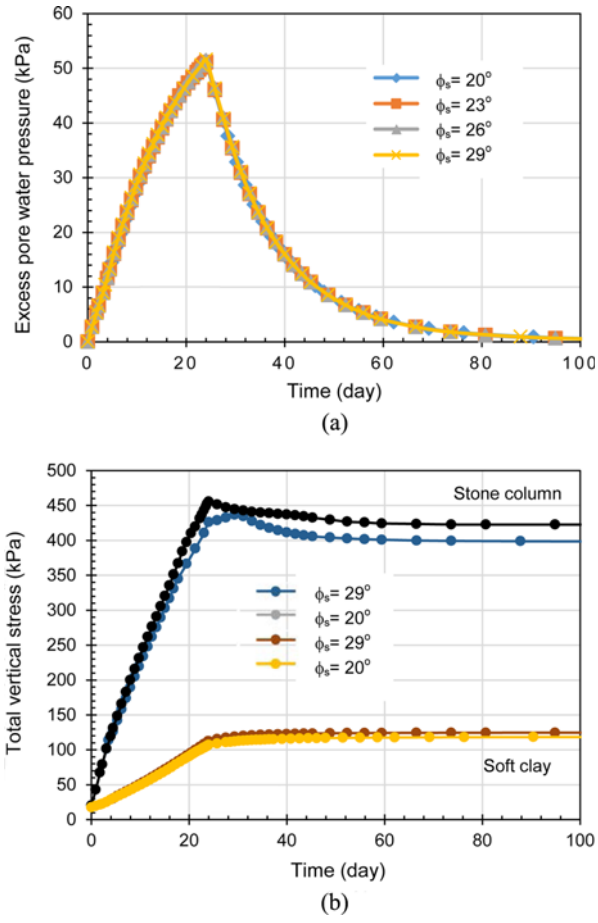

Fig. 11. Effect of Clay Bed Friction Angle on: (a) Excess Pore Water Pressure in the Middle of the Clay Layer, (b) Total Vertical Stresses on Soft Clay and Stone Column

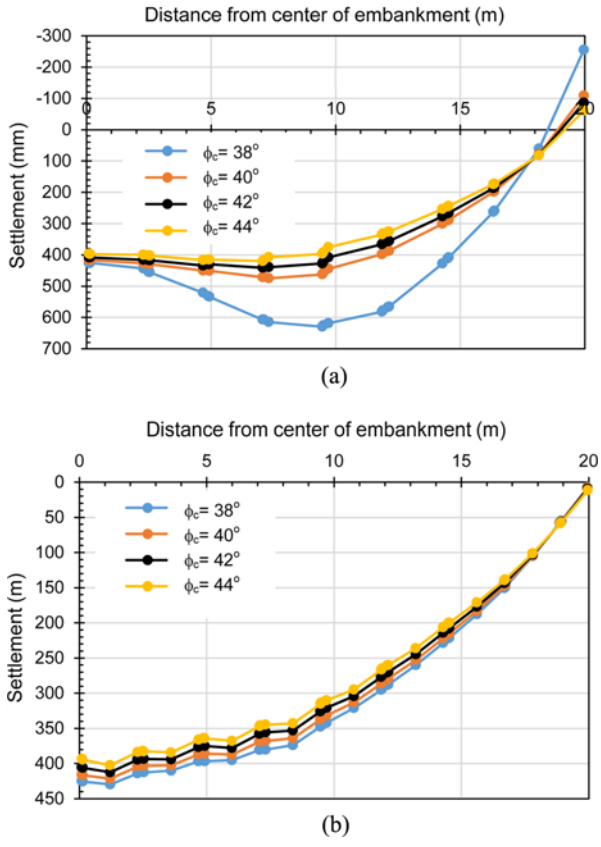

Fig. 12. Effect of Friction Angle of Stone Column Materials on Settlement Profile: (a) Unreinforced Embankment, (b) Reinforced Embankment with Basal Geogrid (J = 4,000 kN/m)

during and after the construction of the embankment. Unsurprisingly, increasing the height of embankment (i.e., construction stages) leads to an increase in total stresses on both the stone column and the surrounding soft soil. As a result of the arching effect, a stress concentration of 3.6 is observed which slowly decreases during the post-construction phase. This can be due to the gain in strength of soft clay during consolidation, which causes the portion of the load transferred to the soft soil to gradually increases thus decreasing the stress concentration ratio. Furthermore, variations of the total vertical stress transferred to the soft clay show that changing the clay friction angle does not alter the stress transferred to the soft clay layer. Subsequently, the excess pore pressure in the middle of the clay layer will remain almost unaffected as observed in Fig. 11(a).

5.3 Influence of the Friction Angle of Stone Column Material (ϕ_c)

Figure 12(a) shows variations of the settlement profile under the unreinforced embankment for different values of the stone column material friction angles. Clearly, increasing the friction angle of aggregates considerably reduces settlement under the unreinforced embankment. For instance, increasing the friction angle from 38° to 44° reduces the maximum settlement by about 33%, i.e., from 625 to 420 mm. Moreover, such an increase has a significant effect on the extent of heave at the embankment toe, in addition to its effects on settlement. Accordingly, increasing the column friction angle from 38° to 44° reduces the heave value from 255 to 85 mm, i.e., 67%.

In contrast, given Fig. 12(b), when the basal geogrid with stiffness of 4000 kN/m is used, the effect of increasing the stone column material friction angle is not significant, as it only reduces the maximum settlement by 8%, i.e., from 38° to 44°. Consequently, the effect of increased stone column material friction angle on reducing the settlement in the unreinforced embankment is far more significant than the reinforced embankment.

The horizontal deformation profile of the foundation soil at the embankment toe for different friction angles of the stone column materials is shown in Fig. 13. According to Fig. 13(a), increasing the friction angle of aggregates remarkably reduces the maximum soil horizontal deformation. For example, when the column friction angle for unreinforced embankment increases from 38° to 44°, the maximum horizontal displacement reduces from 950 to 380 mm, i.e., 60%.

Based on Fig. 13(b), if a high stiffness geogrid is used, the effect of increasing the stone column friction angle on the maximum

soil horizontal displacement will be significantly reduced and becomes roughly negligible. For example, given an embankment reinforced by a geogrid with stiffness of 4,000 kN/m and an increased column friction angle from 38° to 44°, the maximum soil horizontal displacement reduces from 165 to 145 mm.

The remarkable rate of changes in either vertical or horizontal deformations, when ϕ_c varies from 38° to 44° compared to the slight rate of changes when ϕ_c increases from 38° to 40° could be attributed to the significant role of the relative density of stone column material. In the other words, higher density of the column material results a greater portion of the embankment total load to be supported by the column, thus the total stresses transferred to the soft soil and the subsequent deformations decrease.

Unlikely, when embankment is reinforced by a basal geogrid with J = 4,000 kN/m, as shown in Figs. 12(b) and 13(b), any changes in friction angle of the column material, does not cause a significant reduction in settlement nor horizontal deformation. This behavior could be interpreted by the outstanding role of the membrane effect of the basal geogrid which basically leads to a larger part of the embankment load to be reflected onto the tensile force mobilized along the geogrid, which in turn causes the embankment load transferred to the stone column to reduce. Thus, in the case of a reinforced embankment, any changes in the column friction angle do not affect significantly the settlement nor the horizontal deformation of the subsoil.

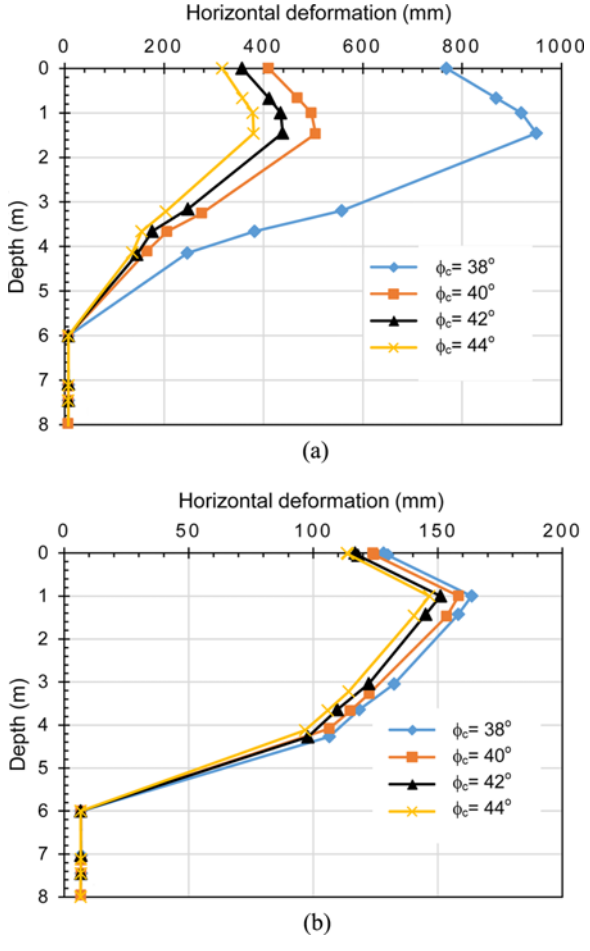

Fig. 13. Profile of Soil Horizontal Deformation under the Embankment Toe: (a) Unreinforced Embankment, (b) Reinforced Embankment (J = 4,000 kN/m)

5.4 Influence of the Stone Columns Length (L_c)

In these analyses, the stone column spacing and diameter are maintained as 2.4 m and 0.8 m, respectively; while their length varies proportionally to the soft clay thickness (H_s) as represented in Table 2. A reinforced embankment is only analyzed here in order to prevent embankment failure owing to given the short length of stone columns.

Figure 14 shows the effect of the stone column length on the settlement profile below the embankment. It is observed that changing the stone column length has a significant effect on the settlement under embankment as well as the heave at the embankment toe. For example, if the column length is changed from $0.25H_s$ to $0.75H_s$, the maximum settlement decreases from 850 to 435 mm. In addition to its effect on the magnitude of settlement, it is observed that such an increase in the stone column length has a considerable effect on the extent of heave at the toe. Accordingly, increasing the column length from $0.25H_s$ to $0.75H_s$ reduces the foundation heave at the embankment toe from 375 to 20 mm, which is nearly 95%.

Figure 15 shows the profile of the soil horizontal deformation beneath the embankment toe for different stone column lengths as well as the geogrid stiffness. According to Fig. 15(a), when the stone column length decreases, the maximum value of subsoil horizontal deformation significantly increases. For example, an increased column length from $0.25H_s$ to $0.75H_s$ reduces the maximum soil horizontal deformation from 2235 to 560 mm, i.e., 75%.

In addition, a direct comparison between the following figures indicates to the significant contribution of the basal geogrid on the maximum soil horizontal deformation. For instance, with a column length of $0.25H_s$ and an increased stiffness of geogrid from 2,000 to 4,000 kN/m, the maximum soil horizontal displacement reduces from 2,235 to 1,085 mm.

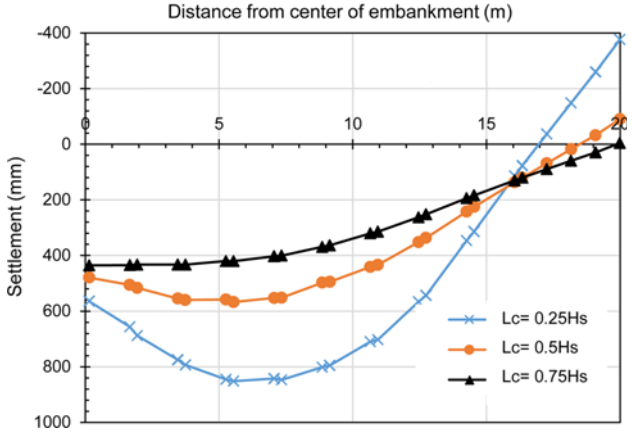

Fig. 14. Settlement Profile under the Reinforced Embankment with a Basal Geogrid (J = 4,000 kN/m)

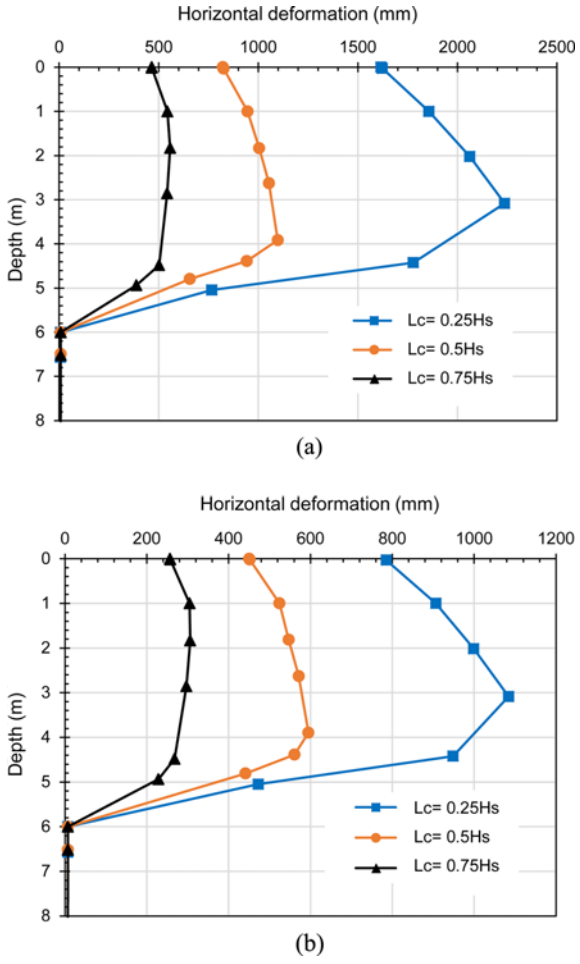

Fig. 15. Profile of the Soil Horizontal Deformation at the Embankment Toe: (a) Reinforced Embankment (J = 2,000 kN/m), (b) Reinforced Embankment (J = 4,000 kN/m)

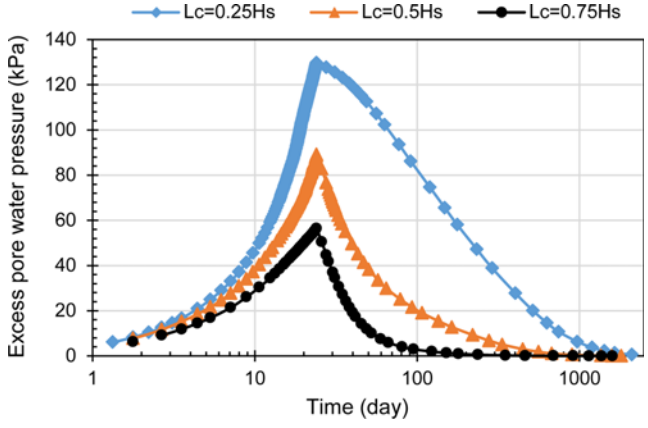

Fig. 16. Changes in Excess Pore Water Pressure in the Center of the Clay Layer (J = 4,000 kN/m)

Figure 16 illustrates the variations of the excess pore water pressure in the middle of the soft clay layer for different stone column lengths. Considering this figure, changing the stone column length has a significant effect on the maximum amount and dissipation of pore pressure. In this regard, changing the column length from 0.25Hs to 0.75Hs reduces the maximum pore pressure from 130 to 57 kPa, i.e., nearly 55%.

Moreover, the figure shows that the longer stone columns hasten the consolidation subsequently reduces the time required for the final settlement. For example, increasing the column length from $0.25H_s$ to $0.75H_s$ reduces the dissipation time from 1,200 to 150 days as a result of the reduction in vertical stresses on the soft clay as well as the increased radial drainage capability, given the increased stone column length.

5.5 Stability Analysis of Embankment

In order to verify the stable performance of the embankment, a c-phi reduction stability analysis was performed to calculate the factor of safety during two consecutive stages: just after load application, and before the next loading stage. Meanwhile, the stability analysis was conducted for unreinforced and embankment reinforced with geogrid with a stiffness of J = 4,000 kN/m. In addition, the influence of the soft clay friction angle on the safety factor of the embankment was studied with the values mentioned in Table 2.

The results of the stability analysis are summarized in Fig. 17 in plots of the factor of safety against the embankment height. Comparing two plots shown in Fig. 17 indicates that the use of the basal geogrid significantly improves the stability of the embankment during both construction and consolidation stages. For example, when using the basal geogrid with stiffness of 4,000 kN/m, the embankment stability improves approximately over 50%, at any stage of load application either consolidation interval.

Regardless of the fact whether or not the basal geogrid is used, the upward trend of the safety factor denotes an increase in the factor of safety during the consolidation interval when the excess pore pressure in the clay layer tends to gradually dissipate, as shown in Fig. 18(b). Afterwards, the value of safety factor critically falls due to rapid load application in saturated clay leading the excess pore pressure to become maximal as illustrated in Fig. 18(a).

The influence of the friction angle of the soft clay under embankment on safety factor is shown in Fig. 19 in which the

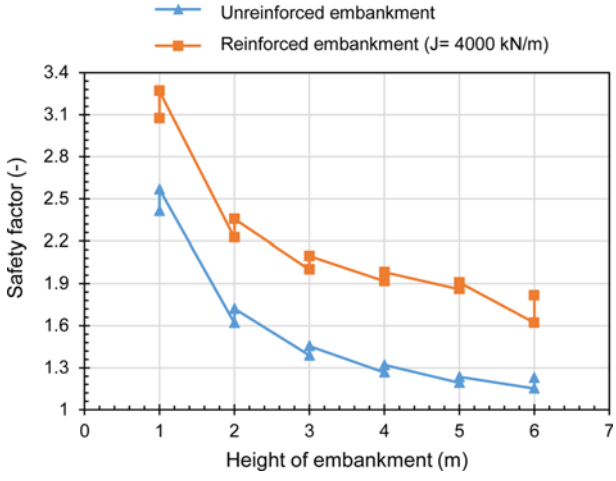

Fig. 17. Influence of Basal Geogrid on Safety Factor of Embankment during Construction and Consolidation Stages

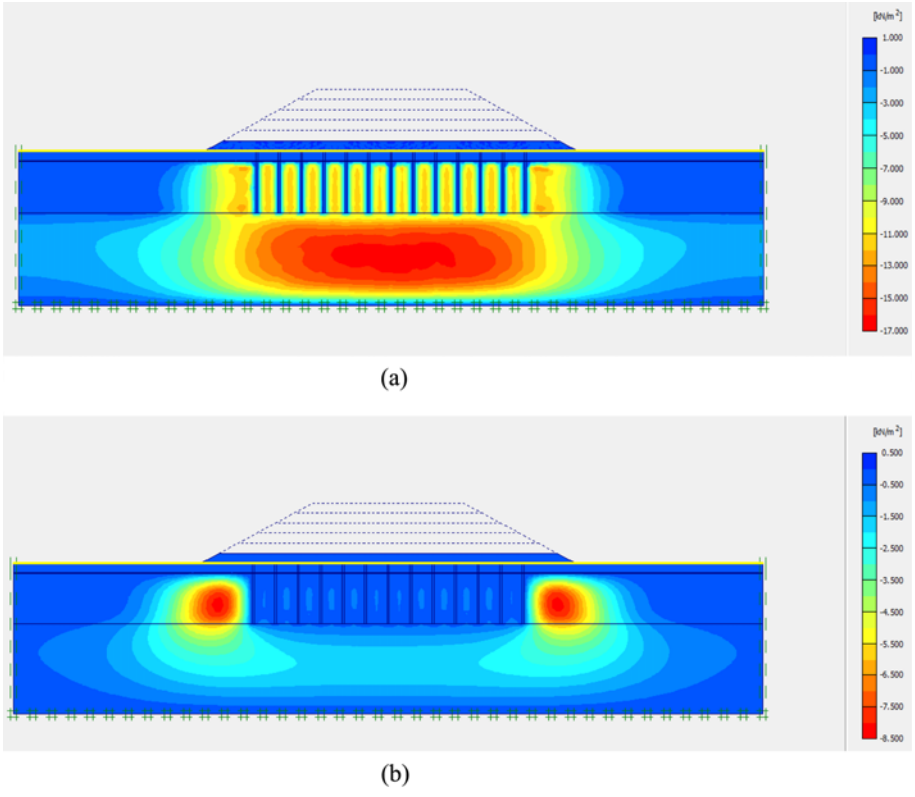

Fig. 18. Distribution of Excess Pore Water Pressure: (a) Immediate after Loading Stage 1, (b) 50 Days after Loading Stage 1

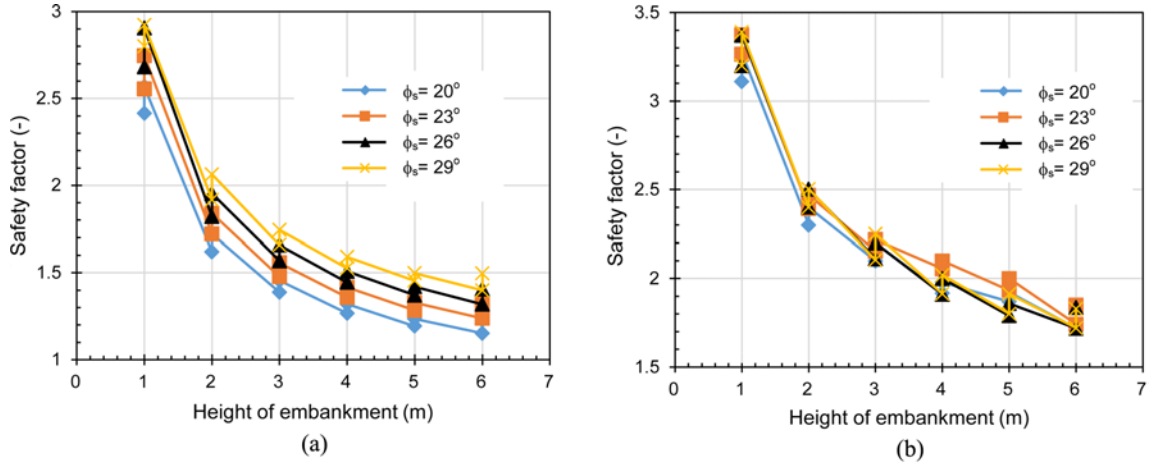

Fig. 19. Influence of Clay Friction Angle on Safety Factor: (a) Unreinforced Embankment, (b) Reinforced Embankment (J= 4,000 kN/m)

variation of the safety factor is plotted against embankment height for different values of the clay friction angle. According to Fig. 19(a), an increase in the friction angle of the soft clay layer leads to an improved factor of safety during both rapid constructions as well as post-construction period. For example, increasing the soft clay friction angle from 20° to 29° causes the ultimate safety factor to improve from 1.2 to 1.5.

Based on Fig. 19(b), for the embankment reinforced by a geogrid with stiffness of 4,000 kN/m, increasing the soft clay friction angle does not significantly affect the stability of the embankment and thus the values of safety factor remain almost unchanged. Consequently, by comparing the following two figures, it can be deduced that the influence of soft clay friction angle on the stability of the embankment depends considerably on whether or not a high stiffness geogrid is placed under the embankment.

6. Conclusions

Plane strain numerical analysis was employed to calculate the behavior of unreinforced and reinforced embankment on soft clay reinforced by stone columns. Following model validation, the effects of parameters such as spacing between stone columns,

basal geogrid stiffness, soft clay friction angle, stone column friction angle, and stone column length were examined. The most significant results are as follows:

1. Results showed that for a constant spacing between the stone columns, using a high stiffness geogrid (i.e., J = 4,000 kN/m) caused to the complete removal of the toe heave and over two times reduction in horizontal soil deformation. That is clear evidence of the great contribution of a high stiffness geogrid in a remarkable reduction of horizontal deformation beneath the embankment.
2. The larger spaced stone columns have shown to increase the settlement under the embankment and the maximum pore pressure in soft clay. However, when the spacing between stone columns reduces from 1.8 m to 2.4 m, the maximum settlement under the embankment reduces about 40% for the unreinforced embankment.
3. An increase in friction angle of the soft clay layer resulted in a significant decrease in embankment settlement and the toe heave, along with a horizontal displacement of the subsoil. This behavior; however, is associated with the stiffness of the basal geogrid. In other words, the contribution of the soft clay properties in embankment behavior is associated with the stiffness of the geogrid layer under the embankment.
4. Increasing friction angle of the aggregates materials caused a significant reduction in the total deformations of the subsoil. Nevertheless, the contribution of the stone column in carrying embankment load reduced as a high stiffness geogrid is placed under the embankment.
5. Change in stone column length has shown to have the highest impact on total deformations and excess pore pressure, among others. It was found that increasing column length from $0.25H_s$ to $0.75H_s$ yields both the vertical and horizontal deformations of soft soil to reduce by about two and five times, respectively. Therefore, embankment stability significantly improves when the stone column length increase from $0.25H_s$ to $0.75H_s$.
6. Stability analysis showed that using a high stiffness basal geogrid causes the embankment short term stability to considerably improve during all stages of construction. As observed, using a geogrid with a stiffness value of 4,000 kN/m, improved the factor of safety from 1.25 to about 1.9 at the end of construction.

Acknowledgments

Not Applicable

Nomenclature

$2b_c$ = Thickness of equivalent shear wall (m)
$2B$ = Influence thickness of equivalent shear wall (m)
c' = Cohesion (kPa)
E_s = Elastic modulus of soft soil (kN/m^2)
E_c = Elastic modulus of stone column material (kN/m^2)
e = Void ratio (dimensionless)
H_e = Height of embankment (m)
H_s = Thickness of soft soil (m)
k_h = Horizontal soil permeability (m/s)
k_v = Vertical soil permeability (m/s)
R = Influence radius of one stone column (m)
r_c = Stone column radius (m)
S = Center to center spacing beyween stone columns (m)
J = Stiffness of geogrid (kN/m)
ϕ_s = Angle of shearing resistance of soft soil (degree)
ϕ_c = Angle of shearing resistance of stone column (degree)
γ = Unit weight of soil (kN/m^3)
υ = Poisson's ratio (dimensionless)
L = Length (m)
ψ = Dilation angle (degree)

ORCID

Ali Ghorbani https://orcid.org/0000-0002-2778-316X
Iman Hosseinpour https://orcid.org/0000-0002-7815-4830

References

Abusharar SW, Han J (2011) Two-dimensional deep-seated slope stability analysis of embankments over stone column-improved soft clay. *Engineering Geology* 120(1-4):103-110, DOI: 10.1016/j.enggeo.2011.04.002

Al-Bared MAM, Harahap ISH, Marto A, Abad SVANK, Ali MOA (2019) Undrained shear strength and microstructural characterization of treated soft soil with recycled materials. *Geomechanics and Engineering* 18(4):427-437, DOI: 10.12989/gae.2019.18.4.427

Al-Bared MAM, Marto A (2017) A review on the geotechnical and engineering characteristics of marine clay and the modern methods of improvements. *Malaysian Journal of Fundamental and Applied Sciences* 13(4):825-831, DOI: 10.11113/mjfas.v13n4.921

Alfaro MC, Balasubramaniam AS, Bergado D, Chai JC (1994) Improvement techniques of soft ground in subsiding and lowland environment. CRC Press, Boca Raton, FL, USA

Almeida MSS, Hosseinpour I, Lima B (2019) Field studies of stone columns and geosynthetic-encased columns. From research to applied geotechnics: Invited lectures of the XVI Pan-American conference on soil mechanics and geotechnical engineering (XVI PCSMGE), November 17-20, Cancun, Mexico, 166

Almeida M, Riccio M, Hosseinpour I, Alexiew D (2018) Geosynthetic encased columns for soft soil improvement. CRC Press, Boca Raton, FL, USA

Barksdale RD, Bachus RC (1983) Design and construction of stone columns, vol. I. Turner-Fairbank Highway Research Center, McLean, VA, USA

Basack S, Indraratna B, Rujikiatkamjorn C (2016) Analysis of the behaviour of stone column stabilized soft ground supporting transport infrastructure. *Procedia Engineering* 143:347-354, DOI: 10.1016/j.proeng.2016.06.044

Brinkgreve RBJ, Vermeer PA (2012) PLAXIS: Finite element code for soil and rock analyses: version 8.5. Balkema, Rotterdam, Netherlands

Cengiz C, Kilic IE, Guler E (2019) On the shear failure mode of

granular column embedded unit cells subjected to static and cyclic shear loads. *Geotextiles and Geomembranes* 47(2):193-202, DOI: 10.1016/j.geotexmem.2018.12.011

Debnath P, Dey AK (2017) Bearing capacity of geogrid reinforced sand over encased stone columns in soft clay. *Geotextiles and Geomembranes* 45(6):653-664, DOI: 10.1016/j.geotexmem.2017.08.006

Elsawy MBD (2013) Behaviour of soft ground improved by conventional and geogrid-encased stone columns, based on FEM study. *Geosynthetics International* 20(4):276-285, DOI: 10.1680/gein.13.00017

Golait YS, Padade AH (2017) Analytical and experimental studies on cemented stone columns for soft clay ground improvement. *International Journal of Geomechanics* 17(4):4016100, DOI: 10.1061/(ASCE)GM.1943-5622.0000779

Greenwood DA (1970) Mechanical improvement of soils below ground surface. Proceedings of ground engineering conference, Institute of Civil Engineering, London, UK

Han J (2015a) Principles and practice of ground improvement. John Wiley & Sons, Hoboken, NJ, USA

Han J (2015b) Recent research and development of ground column technologies. *Proceedings of the Institution of Civil Engineers-Ground Improvement* 168(4):246-264, DOI: 10.1680/grim.13.00016

Hatami K, Bathurst RJ (2005) Development and verification of a numerical model for the analysis of geosynthetic-reinforced soil segmental walls under working stress conditions. *Canadian Geotechnical Journal* 42(4):1066-1085, DOI: 10.1139/t05-040

Hosseinpour I, Almeida MSS, Riccio M (2017a) Verification of a plane strain model for the analysis of encased granular columns. *Journal of Geo Engineering* 12(4):137-145, DOI: 10.6310/jog.2017.12(4).1

Hosseinpour I, Almeida MSS, Riccio, M, Baroni M (2017b) Strength and compressibility characteristics of a soft clay subjected to ground treatment. *Geotechnical and Geological Engineering* 35(3):1051-1066, DOI: 10.1007/s10706-017-0161-8

Hosseinpour I, Mirmoradi SH, Barari A, Omidvar M (2010) Numerical evaluation of sample size effect on the stress-strain behavior of geotextile-reinforced sand. *Journal of Zhejiang University - Science A* 11(8):555-562, DOI: 10.1631/jzus.A0900535

Hosseinpour I, Soriano C, Almeida MSS (2019) A comparative study for the performance of encased granular columns. *Journal of Rock Mechanics and Geotechnical Engineering* 11(2):379-388, DOI: 10.1016/j.jrmge.2018.12.002

Indraratna B, Basack S, Rujikiatkamjorn C (2013) Numerical solution of stone column–improved soft soil considering arching, clogging, and smear effects. *Journal of Geotechnical and Geoenvironmental Engineering* 139(3):377-394, DOI: 10.1061/(ASCE)GT.1943-5606.0000789

Indraratna B, Ngo NT, Rujikiatkamjorn C, Sloan SW (2015) Coupled discrete element–finite difference method for analysing the load-deformation behaviour of a single stone column in soft soil. *Computers and Geotechnics* 63:67-278, DOI: 10.1016/j.compgeo.2014.10.002

Johnson A (2012) Recommendations for design and analysis of earth structures using geosynthetic reinforcements-EBGEO. John Wiley & Sons, Hoboken, NJ, USA

Kadhim ST, Parsons RL, Han J (2018) Three-dimensional numerical analysis of individual geotextile-encased sand columns with surrounding loose sand. *Geotextiles and Geomembranes* 46(6):836-847, DOI: 10.1016/j.geotexmem.2018.08.002

Lima BT, Almeida MSS, Hosseinpour I (2019) Field measured and simulated performance of a stone columns-strengthened soft clay deposit. *International Journal of Geotechnical Engineering* 1-10, DOI: 10.1080/19386362.2019.1653506

Mahawish A, Bouazza A, Gates WP (2018) Improvement of soft soils using bio-cemented sand columns. Proceedings of China-Europe Conference on Geotechnical Engineering, Springer, Berlin, Germany, 822-825

Márcio de Souza SA, Marques MES (2013) Design and performance of embankments on very soft soils. CRC Press, Boca Raton, FL, USA

Mehrannia N, Nazariafshar J, Kalantary F (2018) Experimental investigation on the bearing capacity of stone columns with granular blankets. *Geotechnical and Geological Engineering* 36(1):209-222, DOI: 10.1007/s10706-017-0317-6

Mitchell JK, Huber TR (1985) Performance of a stone column foundation. *Journal of Geotechnical Engineering* 111(2):205-223, DOI: 10.1061/(ASCE)0733-9410(1985)111:2(205)

Mohapatra SR, Rajagopal K (2017) Undrained stability analysis of embankments supported on geosynthetic encased granular columns. *Geosynthetics International* 24(5):465-479, DOI: 10.1680/jgein.17.00015

Muzammil SP, Varghese RM, Joseph J (2018) Numerical simulation of the response of geosynthetic encased stone columns under oil storage tank. *International Journal of Geosynthetics and Ground Engineering* 4(1):4, DOI: 10.1007/s40891-017-0122-6

Najjar SS, Sadek S, Maakaroun T (2010) Effect of sand columns on the undrained load response of soft clays. *Journal of Geotechnical and Geoenvironmental Engineering* 136(9):1263-1277, DOI: 10.1061/(ASCE)GT.1943-5606.0000328

Poorooshasb HB, Meyerhof GG (1997) Analysis of behavior of stone columns and lime columns. *Computers and Geotechnics* 20(1):47-70, DOI: 10.1016/S0266-352X(96)00013-4

Samanta M, Bhowmik R (2019) 3D numerical analysis of piled raft foundation in stone column improved soft soil. *International Journal of Geotechnical Engineering* 13(5):474-483, DOI: 10.1080/19386362.2017.1368139

Sharma RK (2019) A numerical study of granular pile anchors subjected to uplift forces in expansive soils using PLAXIS 3D. *Indian Geotechnical Journal* 49(3):304-313, DOI: 10.1007/s40098-018-0333-3

Tan SA, Oo KK (2005) Stone column FEM modeling — 2D and 3D considerations illustrated by case history. Proceedings of international symposium on tsunami reconstruction with geosynthetics, Asian Center for Soil Improvement and Geosynthetics, December 8-9, Bangkok, Thailand, 157-169

Tan SA, Tjahyono S, Oo KK (2008) Simplified plane-strain modeling of stone-column reinforced ground. *Journal of Geotechnical and Geoenvironmental Engineering* 134(2):185-194, DOI: 10.1061/(ASCE)1090-0241(2008)134:2(185)

Tandel YK, Solanki CH, Desai AK (2012) Reinforced stone column: Remedial of ordinary stone column. *International Journal of Advances in Engineering & Technology* 3(2):340

Vinoth M, Prasad PS, Vittal UKG (2019) Performance analysis of PLAXIS models of stone columns in soft marine clay. Geotechnics for Transportation Infrastructure, Springer, Berlin, Germany, 557-569

Xue J, Liu Z, Chen J (2019) Triaxial compressive behaviour of geotextile encased stone columns. *Computers and Geotechnics* 108:53-60, DOI: 10.1016/j.compgeo.2018.12.010

Zhao L-S, Zhou W-H, Geng X, Yuen K-V, Fatahi B (2019) A closed-form solution for column-supported embankments with geosynthetic reinforcement. *Geotextiles and Geomembranes* 47(3):389-401, DOI: 10.1016/j.geotexmem.2019.01.006